Journal of International Scientific Publications: Materials, Methods and Technologies

Volume 8, ISSN 1314-7269 (Online), Published at: http://www.scientific-publications.net

THERMAL CONDUCTIVITY IN IMPROVEMENT OF SAFETY OF NUCLEAR FUEL

B. Szpunar[a,*], J.A. Szpunar[b]

[a]Department of Physics and Engineering Physics, University of Saskatchewan, Saskatoon, SK S7N 5E2, Canada

[b]Department of Mechanical Engineering, University of Saskatchewan, Saskatoon, SK S7N 5A9, Canada

Abstract

We investigate thermo-mechanical properties of alternative fuels like thoria and uranium nitride up to a very high temperatures (ThO_2: 3300 K, UN: 3000 K). We demonstrate that, by combining first-principles quantum-mechanical calculations with classical correlations, it is possible to predict thermal properties in agreement with experiment. The new generalized gradient approximation functional within the density functional theory predicts, in agreement with experiment, not only mechanical properties but also the absolute values of the lattice constant of thoria. The main contribution to the thermal conductivity of thoria (lattice) and uranium nitride (electronic) are evaluated in a wide range of temperatures.

1. INTRODUCTION

The recent tragic accident in Fukushima clearly illustrates the risks associated with the present design of reactors based on uranium dioxide fuel and justifies the research towards a safer fuel. The previous studies by Pioro et al. [49] demonstrate that the traditional urania fuel is not suitable for some design of new generation reactors due to its low thermal conductivity (e.g. the estimated fuel centerline temperature for SuperCritical Water reactor (SCWR) surpasses the industry accepted limit of 1850°C). Therefore uranium nitride (UN) is considered as a possible safer fuel and we present here a preliminary studies of its thermal conductivity. At the time of increasing cost of traditional urania fuel, it is more economically justified to look at the alternative fuels like thoria, which is four times more abundant. Thoria is also regarded as a fuel for safer reactors as it has a higher thermal conductivity (for most temperatures of interest) and melting point [2] than urania, which prevents reactor melt down. However in contrast to urania that has been studied extensively, because it has been used in nuclear reactors as a fuel for a long time, there are only limited experimental data available for thoria as reviewed in Ref. [2]. Although thoria fuel has been investigated for some time [2] its high temperature thermo-mechanical properties, needed for nuclear safety analysis, are not available. Therefore in this work, we present an attempt at applying *first-principles* calculations to evaluate the high temperature thermo-mechanical properties of thoria.

In Ref. [3], we presented the first-principles calculations of the lattice constants of thoria at 0 K temperature, using CASTEP code [4]. We noted that the generalized gradient approximation (GGA) framework with the early [5,6] implementation led to significantly overestimated bond length and underestimated bulk moduli [7,8] while local density approximation LDA [9] significantly underestimated lattice constants.

The present paper applies the density functional theory (DFT) using the new GGA implementation (WC [10]) to evaluate structural and thermo-mechanical properties of thoria.

2. EVALUATION OF THE PROPERTIES OF THORIA AT 0 K TEMPERATURE

We present here the new results (Table 1), which demonstrate that the more recently proposed GGA: WC [10] and PBEsol [11] lead to improved lattice constant values, with bulk (B) modulus in agreement with experiment (Table 2). We used the Monkhorst-Pack 13×13×13 grid of special k-points [12] and a cut-off energy of 610 eV.

Thoria has a cubic structure ($Fm\bar{3}m$ symmetry) and therefore one strain pattern (with only xx and yz non-zero) is enough to calculate all elastic moduli [15]. Four values for the amplitude of the strain were applied: ± 0.3%, ± 0.1%.

We calculated the values of bulk (B) and shear (G) modulus as the Hill averages of the obtained by Voigt [16] and Reuss [17] methods. Having calculated the bulk and shear modulus, Young's modulus (Y) can be evaluated for an isotropic material or an isotropic aggregate of grains with non-isotropic elastic properties as:

$$Y = \frac{9BG}{3B + G} \quad (1)$$

Additionally, Young's modulus is calculated in <100> cubic symmetry directions from a reciprocal of the respective (s_{11}) compliance ($Y_{[100]} = s_{11}^{-1}$).

The Poisson's ratio is calculated as:

$$\eta = \frac{3B - 2G}{2(3B + G)} \quad (2)$$

Table 1

Lattice constants of thoria calculated using CASTEP [4] and various functionals as indicated.

Method	Lattice constant (a) [Å]
LDA [9]	5.53
PBE [6]	5.61
PBEsol [11]	5.55
WC [10]	5.56
Experiment	5.598 [13]
	5.600 [14]

Table 2

Elastic moduli, elastic constants (stiffness values) and Poisson's ratio of thoria calculated versus experimental measurements

Property	ThO_2			
(in GPa; # unit-less)	(PBE) [6]	(PBEsol)	(WC) [10]	Experiment (fully dense)
B	187.6	202.8	203.0	193 [18,19] 223 [20]
G	85.4	96.6	96.4	100.1, 100.8 [21] 97.2 [18]
Y ($Y_{(x,y)}$, $Y_{(z)}$)	222.4 (303.4)	250.1 (313.3)	249.7 (312.5)	262.1, 260.6 [21] 247.7 [18]
c_{11}	351.9 ($\pm$ 2.1)	370.9 ($\pm$ 1.9)	370.6 ($\pm$ 1.2)	377 [20] 367 [19]
c_{12}	105.4 ($\pm$ 1.4)	118.7 ($\pm$ 1.4)	119.3 ($\pm$ 0.8)	146 [20] 106 [19]
c_{44}	70.9 ($\pm$ 0.4)	80.8 ($\pm$ 0.3)	80.7 ($\pm$ 0.3)	89 [20] 79 [19]
$n\eta$	0.30	0.29	0.30	0.301 [21] 0.284 [18]

As indicated, Table 2 shows the compared results for various GGA functionals. The mechanical moduli, calculated using WC and PBEsol GGA functionals, show much better agreement with experimental result [18-21] for ThO_2 than the underestimated values by PBE.

3. INVESTIGATION OF THORIA AT UP TO 3300 K TEMPERATURES

In this section we will use combination of first principles calculations and extrapolated to high temperatures correlations, derived from experimental data, to evaluate thermal properties of thoria up to 3300 K.

3.1. Thermal expansion

In order to examine the thermal expansion of thoria, we have performed preliminary *first-principles* molecular dynamics (MD) simulations using an Andersen-Hoover barostat [22,23]. The unit cells used, although eight times larger than conventional unit cells (96 total number of atoms), with periodic boundary condition were still small and therefore we observed large thermal fluctuations at higher temperatures. We did the calculations for 4 ps (5.5 ps for 3300 K) and the time-step of 0.001 ps. We reduced the grid for k points for this super-cell to 2×2×2. We made the calculations for selected temperatures (starting at 273 K) and constant pressure [24] (1 atm). Fig. 1 shows the running averages of the lattice constants simulated by CASTEP (WC functional) molecular dynamics as a function of temperature and indicated by open red squares. The calculated lattice constants of thoria agree well with experimental data by Mathews et al. [25] (Fig. 1). Evaluation of the thermo-mechanical properties of thoria using the theoretical thermal expansion was done previously in Ref. [26]. In Ref [27] the relative thermal expansion of thoria is provided for a wide temperature range (up to 2755 K (4500 F)) and it was used in the calculation of the lattice constants of thoria (shown in Fig. 1 by black spheres) with the assumed value at 0 K equal to 5.56 Å (the value obtained using WC as presented in Table 1). The temperature (T) dependence of the respective lattice constants (a in Å) is described well (R^2 = 0.999) by a parabolic fit (indicated by a solid black line in Fig. 1):

$$a(T) = a_0(1+9.899347\times10^{-10}T^2 + 7.859124\times10^{-6}T - 2.465599\times10^{-3}) \quad (3)$$

Eq. 3 was also used to calculate values of the lattice constants at 3000 K and 3300 K, shown by white spheres in Fig. 1. Since the extrapolated experimental data from Ref. [27] predict lower values of the lattice constants at higher temperatures, it is of interest to calculate thermo-mechanical properties of thoria using these data.

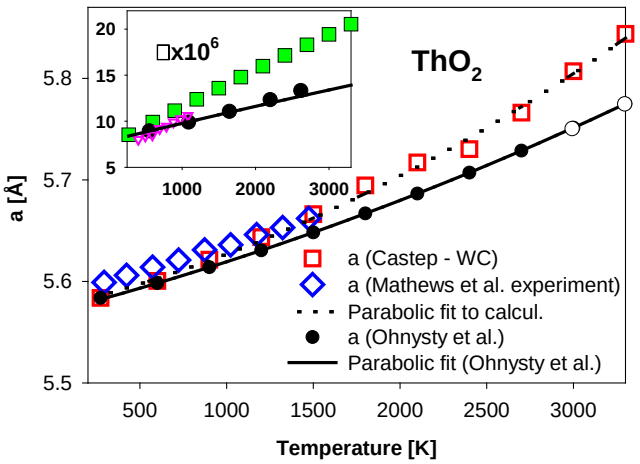


Fig. 1. The calculated lattice constant of thoria as a function of temperature (open squares) is shown versus experimental data (open diamonds) [25]. The solid line shows the parabolic fit (Eq. 3) to the calculated data. In the insert, the derived (Eq. 4) linear thermal expansion coefficient (α) is shown (filled green squares) versus experimental points (filled black circles [27] and blue triangles [28]).

The linear thermal expansion coefficient ($\alpha_p(T)$) can be derived from Eqs. 3 and 4:

$$\alpha(T)_P = \frac{1}{L}\left(\frac{\partial L}{\partial T}\right)_P \quad (4)$$

The calculated linear thermal expansion coefficient, shown in the insert in Fig. 1 by solid black line, has linear temperature dependence similar to the coefficient evaluated from the recently published [29] parabolic correlation for a linear thermal expansion of thoria with 3.45 wt. % UO_2 for temperatures up to 1473 K. The black spheres indicate provided in Ref. [27] average values for the linear thermal expansion coefficient. They are in agreement with the derived values from the parabolic fit (Eq. 3). However CASTEP calculations using WC functional predict slightly larger linear thermal expansion above 900 K than experimentally reported [27] and as discussed in details before [30], although it is predicted to be lower above 1800 K than recommended by Fink data for urania [31]. The evaluated slope of ~ $1.98\times10^{-9}K^{-2}$ (Eq. 3) is lower than predicted from MD ~$3.99\times10^{-9}K^{-2}$ and the observed one at the lower temperature [28] (see insert in Fig. 1) ~$3.96\times10^{-9}K^{-2}$. The previous quasi-harmonic approximation (QHA) calculations of thoria thermal expansion (done at lower temperatures) were lower and, for example, at 1100 K the reported values are 10.1×10^{-6} K^{-1} [32] and 10.7×10^{-6} K^{-1} [33] versus MD 11.9×10^{-6} K^{-1}. The experimental values shown in the insert are for 9.9×10^{-6} K^{-1} at 1088.706 K [27] and 10.6×10^{-6} K^{-1} at 1080 K [28]. It has to be noted that the calculations are done for a fully dense bulk, ideal structure, which is not the case in reality, therefore we will use here lattice constants evaluated from Eq. 3.

a. Mechanical properties

Knowledge of the lattice constants as a function of temperature allows the derivation of the adiabatic elastic moduli (c_{ij}) defined as [34]:

$$c_{ij_S} = (\partial^2 U / \partial\varepsilon_i \partial\varepsilon_j)_{S,\varepsilon} \quad (5)$$

where U is internal energy, S is entropy and $\varepsilon_{i(j)}$ is strain. Four values for the amplitude of the strain were applied: ± 0.3%, ± 0.1% at the selected temperatures as well as for the respective lattice constants as calculated from Eq. 3 and shown in Fig. 1. Next we calculated the adiabatic Young, share moduli, and compressibility as the Hill averages of the obtained values by Voigt [16] and Reuss [17] methods, as described above. We calculated the Young modulus in <100> directions using a reciprocal of the respective (s_{11}) compliance.

Figs. 2 and 3 show the Young and shear moduli, together with compressibility (ß) as a function of temperature (0-3300 K) for the respective lattice constants, shown in Fig. 1. Additionally we include for comparison the experimental points for thoria and urania as selected in Ref. [2]. Both oxides show similar behaviour of mechanical properties with temperature, and good agreement with experimental results and the calculated data.

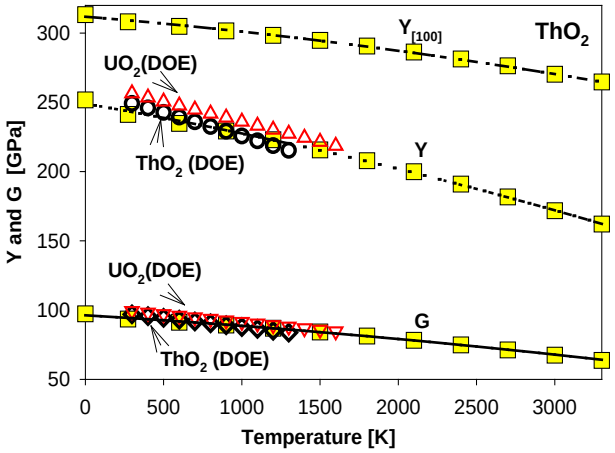


Fig. 2. The calculated adiabatic Young (Y and Y[100]) and shear (G) moduli of thoria as a function of temperature (yellow filled squares) versus experimental data (open circles and diamonds) [2] Additionally, the respective experimental data are shown (red triangles) for urania [2].

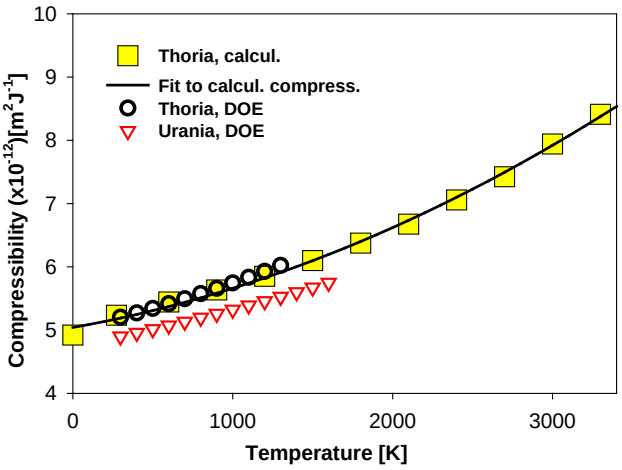


Fig. 3. The calculated adiabatic compressibilty of thoria as a function of temperature (yellow filled squares) is shown versus experimental data (open circles) [2]. The measured compressibility for urania [2] is indicated by red triangles for comparison.

The equations for the curves fitted to the calculated data, shown (black lines) in Figs. 2 and 3 as a function of temperature (T in K), are (R^2 = 0.998 for Y, $Y_{[100]}$, G and 0.997 for β):

$$Y = -2.1\times10^{-6}T^2 - 0.01935T + 248.91 \quad (6)$$

$$Y_{[100]} = -1.5\times10^{-6}T^2 - 0.0093T + 311.79 \quad (7)$$

$$G = -0.9\times10^{-6}T^2 - 0.0068T + 96.275 \quad (8)$$

$$ß = 1.7\times10^{-7}T^2 + 0.00045T + 5.0406 \quad (9)$$

where Young (Y and Y[100]) and shear (G) moduli are in GPa, and compressibility (β $\times10^{-12}$) in m^2J^{-1}, respectively. Fig. 2 shows that the Young moduli in the principal crystallographic directions are not only larger but also less dependent on temperature than the calculated Young modulus for polycrystalline thoria with random texture.

3.3. Thermal conductivity

It was noted previously [32,33] that the phonon contribution to the thermal conductivity of thoria can be well reproduced using a simplified Slack model [35]. Here we extend this application to higher temperatures (up to 3300 K) using the thermal expansion (α(T), a(T)) and the adiabatic elastic moduli evaluated above.

Next we calculate the Grũneisen parameter from:

$$\gamma(T) = \frac{3\alpha(T)V_M(T)}{C_V(T)\beta(T)} \quad (10)$$

where $V_M(T)$ is molar volume and $C_V(T)$ is the heat capacity at constant volume per mol.

The heat capacity can be obtained from [36]:

$$C_v(T) = N_A k_B \int_{\omega_{min}}^{\omega_{max}} \frac{\left(\frac{\hbar\omega}{k_BT}\right)^2 \exp\left(\frac{\hbar\omega}{k_BT}\right)}{\left[\exp\left(\frac{\hbar\omega}{k_BT}\right)-1\right]^2}\rho(\omega)d\omega \quad (11)$$

where N_A is Avogadro number, k_B is the Boltzman constant and $\rho(\omega)$ is the density of states of phonons (with $\hbar\omega$ energy) per primitive unit cell (ThO_2). Note that heat capacity at constant volume remains constant at

higher temperatures. We assume also that it stays flat for 3000 K and 3300 K when evaluating the Grũneisen parameter at these high temperatures.

The Poisson's ratio (η) at these selected temperatures can be evaluated by Eq. 2 using the calculated shear and Young moduli (presented in Fig. 2). Next we evaluate the scaling function [37]:

$$f(\eta) = 3^{1/3}\left[2\left(\frac{2}{3}\frac{1+\eta}{1-2\eta}\right)^{3/2} + \left(\frac{1}{3}\frac{1+\eta}{1-\eta}\right)^{3/2}\right]^{-1/3} \qquad (12)$$

This allows us to evaluate the Debye temperature (θ in K) within the isotropic approximation [37] (in atomic units: m= $\hbar$ = e = 1):

$$\theta(T) = \frac{\left(6\pi^2 V(T)^{1/2} n\right)^{1/3} f(\eta(T))}{k_B(\beta(T)M)^{1/2}} \qquad (13)$$

(s deleted in formulas) where the same notation as above is used and n is the number of atoms per primitive cell (3 for ThO_2) with its volume V(T) (calculated using a(T) derived above) and mass M.

Now we can evaluate the lattice thermal conductivity ([35,32], note a typo in the respective Eq. 8 in Ref. [33]):

$$\kappa_L = \frac{(1-0.05)^{1.5} C\theta(T)^3 M_M V(T)^{1/3}}{(n\gamma(T))^2 T} \qquad (14)$$

where C is equal to 3.04×10^4 $Wm^{-2}K^{-1}$ g^{-1} mol and M_M molar mass per primitive cell (264 g mol^{-1} for ThO_2) and V(T) is as above, the volume of the primitive cell, but in cubic m. The first factor in the numerator is accounting for assumed 5% porosity. The measured thermal conductivity data were critically reviewed in Ref. [38], corrected to 95% TD and fitted (for the temperature (T) range 300-1700 K) to the following equation (with the numerator accounting for 5% porosity):

$$\kappa_{inv}^{95\%}(T) = \frac{(1-0.05)^{1.5}}{A + BT} \qquad (15)$$

where A and B are constants associated with phonon-defects (A) and phonon-phonon (B) scattering contribution to the mean path and the respective values of lattice thermal conductivity are displayed in Fig. 4 by blue triangles.

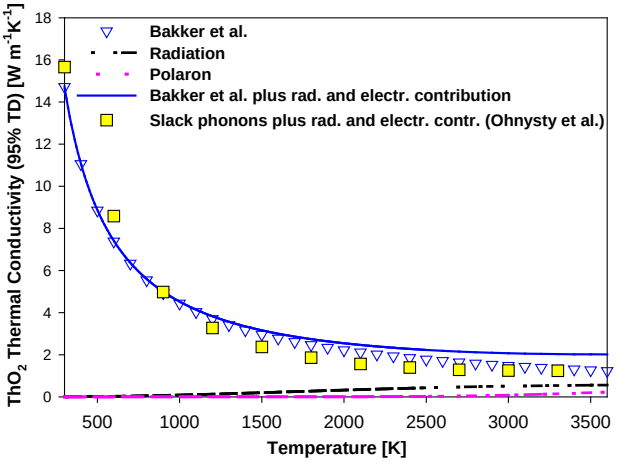


Fig. 4. The calculated thermal conductivity of thoria (95% TD) as a function of temperature. The blue triangles show the phonon contribution [38]. The radiative and electronic contributions [39] at high temperature for thoria are indicated by dashed medium black and dashed long pink lines, respectively. The solid blue line represents the total thermal conductivity with the phonon contribution described by Eq. 15 and the parameters derived in Ref. [38]. The yellow squares indicate the lattice thermal conductivity derived from Eq. 14 plus radiative and electronic contribution from Ref. [39]..

At higher temperatures (up to the melting point), as evaluated previously [39], the radiation contribution to the thermal conductivity becomes visible as also shown by the medium dashed black line, while the electronic contribution is relatively small due to a large band gap of thoria. As discussed before [39], when all contributions to the thermal conductivity (including phonon contribution described by Eq. 15 extended to high temperatures) are added together, the thermal conductivity becomes flat (as indicated by solid blue line) approaching the value around 2 $Wm^{-1}K^{-1}$ in agreement with Fig. 6.24 in Ref. [2] and with the value 2.5 $Wm^{-1}K^{-1}$ reported in Ref. [40], where Hyland notes that this thermal conductivity is maintained up to the melting temperature. In Fig. 4 we also show by yellow squares the respective 95% TD total thermal conductivity with phonon contribution evaluated from Eq. 14. Although agreement with experiment is good up to around 1000 K at higher temperatures the thermal conductivity is under-predicted.

Our analysis indicate that lattice thermal conductivity decreases rapidly with increasing temperature and therefore as indicated previously (e.g. in Ref. [1]) ceramic fuels like thoria and urania are not suitable as a fuel for the nuclear reactors that operate at very high temperatures.

4. THERMAL CONDUCTIVITY OF UN

We have shown that the thermal conductivity of ceramic fuels is low at higher temperatures, therefore in this section we will discuss exemplary case of metallic fuel. We will investigate here the recommended for SCWR uranium nitride [1], since it has high electronic contribution to the thermal conductivity that increases with temperature.

4.1 Electronic structure

The electronic structure of UN has been studied before (see e.g. [41,42]) and it was noted that neither LDA or LDA with Hubbard U corrections are capable to describe well its electronic structure around Fermi energy that is dominated by strongly correlated 5f electrons of uranium with antiferromagnetic ordering.

Similarly to thoria UN has cubic structure ($Fm\bar{3}m$ symmetry). However at low temperatures (below Néel temperature T_N = 53 K [43]) it shows ferromagnetic (001) planes coupled antiferromagnetically (type-I structure) [43]. We have discussed previously [3] that the calculated lattice constants for ferromagnetic urania agreed very well with experiment while for antiferromagnetic ordering very close values of the lattice constants were found but with unphysical, slight tetragonal distortion. It is much easier to optimize geometry of ferromagnetic UN due to smaller size of the primitive unit cell. Using Quantum Espresso code [44] and PBE functional [6] we have found the equilibrium lattice constant for ferromagnetic UN to be 5.24 Å, which is larger than experimental value of 4.89 Å [43] since PBE overestimates lattice constants values. The used norm conserved potentials provided with Quantum Espresso code (pbe-mt_fhi.UPF) may also lead to a larger lattice constant. 300 Ry cut off energy and 16×16×16 k points mesh in the Brillouin zone was applied. It was tested that changing cut off energy up to 75 Ry and changing grid up to to 10×10×10 have not affected the lattice constant.

Next we performed band structure calculation for antiferromagnetic and nonmagnetic UN using conventional unit cells (with 5.24 Å lattice constant) and no symmetry. We used 150 Ry cut of energy and the Monkhorst-Pack [12] 16×16×16 grid to calculate the electron band structure suitable as an input to BoltzmannTransportProperties (BoltzTraP) code [45]. The BoltzTraP code uses smooted Fourier interpolation of the electron band structure, which is used to calculate the electron density of states and semiclasic transport coefficients [45]. In Fig. 5 the derived electron densities of states (black, solid lines) and theirs integrals over energy (dashed red lines) are shown for antiferromagnetic (a) and nonmagnetic (b) UN, respectively. In the nonmagnetic calculations one broad peak originated from 5f electrons is visible (b) near the Fermi energy, which splits into two peaks for antiferromagnetic ordering (a).

In BoltzTraP code it is assumed that the electron relaxation time is isotropic and constant. which is true at lower temperatures where residual resistivity is dominant. We evaluated the relaxation time ($\tau = 4.98\times10^{-15}$s) using the calculated by BoltzTraP (for non-magnetic UN) at 300 K electronic conductivity, σ/τ equal to 1.18875×10^{20} $\Omega^{-1}m^{-1}s^{-1}$ and the measured resistivity at the same temperature: 16.9×10^{-7} Ωm [41]. However since the neglected in BoltztraP the lattice resistivity increases linearly with temperature it becomes important at high temperatures. We evaluated this contribution from the experimental resistivity slope between 300 K and 1100 K [46] and included it in the evaluation of thermal conductivity. The presented in Fig. 6 the electronic contributions to the thermal conductivity of UN (black, solid line for non-magnetic UN and short, dashed, black line for non-

magnetic UN with taken into account correction for lattice resistivity) were calculated via Wiedemann-Franz law from the electronic conductivities:

$$\kappa_e = \frac{\pi}{3}\left(\frac{k_B}{e}\right)^2 \sigma \qquad (16)$$

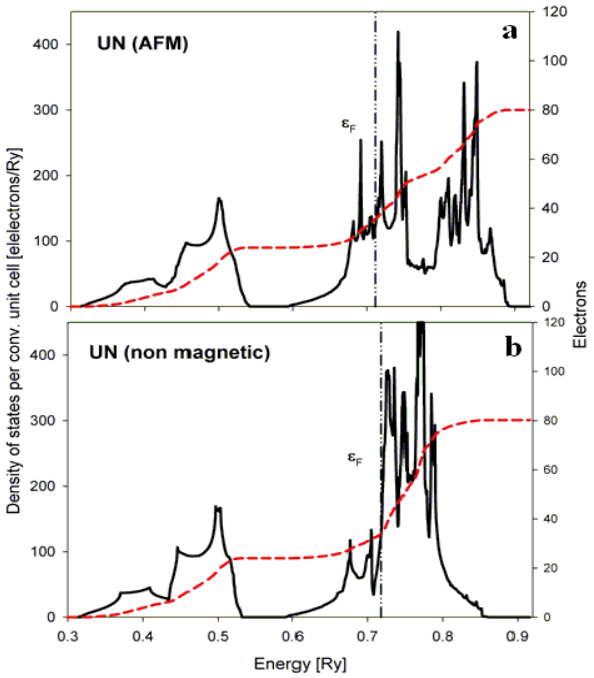


Fig. 5. The calculated total (black, solid line) electron density of states of UN using PBE functional for antiferromagnetic (a) and nonmagnetic (b) state and conventional unit cell. The integrated over energy densities of states are shown by red dashed lines.

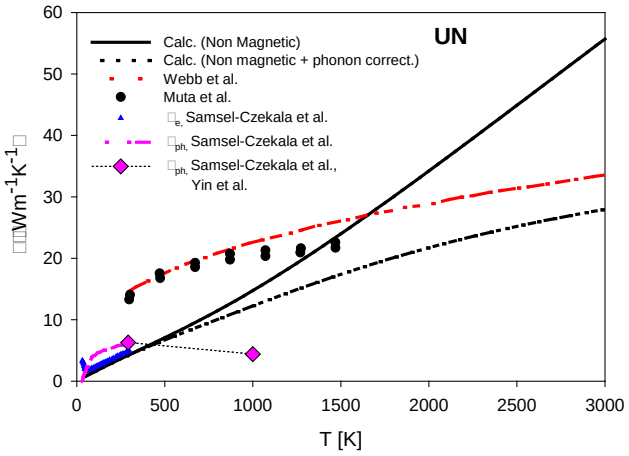


Fig. 6. The calculated thermal conductivity of electronic origin in UN as a function of temperature are shown for antiferromagnetic (black solid line) and nonmagnetic state (short, black, dashed line). The previously estimated phonon contribution to the thermal conductivity at 1000 K [42] is indicated by pink diamond and at lower temperatures by pink dashed line [41]. The dotted line indicates the phonon contribution evaluated by the linear interpolation between the estimates from Refs. [41] and [42]. The calculated from the experimental resistivity the electronic contribution [41] is shown by blue triangles. The measured total thermal conductivity is indicated by long, red, dashed line [47] and black spheres [48].

The previously estimated electronic thermal conductivity [41], shown by blue triangles in Fig. 6, is in a very good agreement with the calculated here values for non-magnetic UN and above Néel temperature (51 K). The phonon's contribution to the thermal conductivity (indicated by dashed and dotted pink lines) decreases with temperature and therefore around 1500 K our estimate of the electronic contribution to the thermal conductivity of non-magnetic UN (black solid line) agrees well with the measured thermal conductivity (long, red, dashed line [47] and black spheres [48]). However the over-prediction of the thermal conductivity at higher temperature makes questionable the assumption used in BoltzTraP that the relaxation time is constant for the whole range of temperatures and therefore we also included the thermal conductivity calculated using the correction for the lattice resistivity (short, dashed black lines). There is however disagreement between experimental data for a resistivity (e.g. at 300 K: 16.9×10^{-7} Ωm [41] versus 14.8×10^{-7} Ωm [46]) and also the thermal conductivity as shown in Fig. 6 (e.g. around 1500 K: 22 $Wm^{-1}K^{-1}$ [48] versus 26 $Wm^{-1}K^{-1}$ [47]). The band structure of uranium 5f electrons is also not very well represented within DFT, as discussed before [42]. However our calculations reproduce very well the trend for the increasing with temperature the thermal conductivity of UN.

5. SUMMARY

In summary, since the calculated thermo-mechanical properties of thoria, presented here are in good agreement with available low temperature experimental data, one can assume that the predicted properties at high temperatures can be used as complementary data before experiments are available.

We demonstrate that, by combining first-principles quantum-mechanical calculations with classical correlations, it is possible to predict thermal properties of in agreement with experiment. In particular the calculations demonstrate that thoria fuel, although it has higher thermal conductivity than urania at the typical operating temperatures of conventional nuclear reactors, is not suitable as a fuel at high temperatures. The metallic fuels like UN show high electronic contribution to the thermal conductivity, which increases with temperature and therefore it makes it more suitable as a fuel for some new generation reactors like for example SCWR.

ACKNOWLEDGEMENTS

The authors acknowledge access to high performance supercomputers at CLUMEQ, Westgrid and Plato and collaboration with Ki-Seob Sim on thoria and I.L. Pioro on UN fuel.

The authors are also grateful to Ming-Hsien Lee for providing normconserving pseudopotentials for thorium and oxygen that were used in this work.

REFERENCES

[1] I.L. Pioro, M. Khan, V. Hopps, Ch. Jacobs, R. Patkunam, S. Gopaul, and K. Bakan, JSME J. of Power and Energy Systems, 2 (2008) pp. 874-888.

[2] Thorium dioxide: properties and Nuclear Application, (J. Belle and R.M. Berman (Ed.), Washington, D.C.) DOE-NE-0060 (1984) p591 p.

[3] B. Szpunar, J.A. Szpunar, J. Nucl. Mater, 439, (2013) 243-250.

[4] M.D. Segall, P.L.D. Lindan, M.J. Probert, C.J. Pickard, P.J. Hasnip, S.J. Clark and J.D. Payne, J. Phys. Condens. Matter 14 (2002) 2717-43.

[5] J.P. Perdew, Y. Wang, Phys. Rev. B45 (1992) 13244-9.

[6] J.P. Perdew, K. Burke, M. Ernzerhof, Phys. Rev. Lett. 77 (1966) 3865-8.

[7] A.D. Corso, A. Pasquarello, and A. Baldereschi, Phys. Rev. B53 (1996) 1180-5.

[8] X. Zhao and D. Vanderbilt, Phys. Rev. B65 (2002) 075105-10.

[9] D.M. Ceperley, B.J. Alder, Phys. Rev. Lett. 45 (1980) 566-9.

[10] Wu A., Cohen R.E., Phys. Rev. B, 73 (2006) 235116 (6pp) .

[11] J.P. Perdew, A. Ruzsinszky, G.I. Csonka, O.A. Vydrov, G.E. Scuseria, L.A. Constantin, X. Zhou, K. Burke, Phys. Rev. Lett. 100 (2008) 136406 (4pp); 102 (2009) 039902(E).

[12] H.J. Monkhorst and J.D. Pack, Phys. Rev. B 13 (1976) 5188-92.

[13] J.S. Olsen, L. Gerward, V. Kanchana, G. Vaitheeswaran, J. Alloy. Compd. 381 (2004) 37-40.

[14] M. Idiri, T. Le Bihan, S. Heathman, J. Rebizant, Phys. Rev. B 70 (2004) 014113-9.

[15] J.F. Nye, Physical Properties of Crystals, Oxford University Press, 1990, p329.

[16] W. Voigt, in: B.G. Teubner,(Ed.) Lehrbuch der Krystallphysik, p.962, Leipzig.

[17] A. Reuss, Z. Angew. Math. Mech. 9 (1929).49-58.

[18] K.K. Phani, D. Sanyal, J. Eur. Ceram. Soc. 29 (2009) 385-90.

[19] P.M. Macedo, W. Capps, J.B. Watchman, J. Am. Ceram. Soc. 47 (1964) 651-1.

[20] K. Clausen, W. Hayes, J.E. Macdonald R. Osborn, P.G. Schnabel, M.T. Hutchings, A. Magrel, J. Chem. Soc., Faraday Trans. 83 (1987) 1109-1117.

[21] K.K. Phani, J. Matt. Sc. Lett. 5 (1986) 747-59.

[22] H.C. Andersen, J. Chem. Phys., 72 (1980) 2384-93.

[23] W. Hoover, Phys. Rev. A31 (1985) 1695-7.

[24] S. Nosé, Progr. of Theor. Phys., Suppl., 103 (1991) 1-46.

[25] M.D. Mathews, B.R. Ambekar and A.K. Tyagi, J. Nucl. Mater. 280 (2000) 246-9.

[26] B. Szpunar B and J.A. Szpunar, Proc. of the 19th Pacific Basin Nuclear Conference, Vancouver, August 24-28th, (2014), PBNC1014-124.

[27] B. Ohnysty and F.K. Rose, J. Am. Ceram. Soc. 47 (1964) 398-400.

[28] D. Taylor, Br. Ceram. Trans. J., 83 (1984) 32-7.

[29] R.K. Bhagat, K. Krishnan, T.R.G. Kutty, A. Kumar, H.S. Kamath, S. Banerjee, J. Nucl. Mat., 422 (2012) 152-7.

[30] B. Szpunar, ATINER'S Conf. Paper Series, No: PHY2013-0527, ISSN 2241-2891, (Athens, 2013).

[31] J.K. Fink, J. Nucl. Mater. 279 (2000) 1-18.

[32] H.Y. Xiao, Y. Zhang, W.J. Weber, Acta Materialia 61(2013) 467-76.

[33] Y Lu, Y Yang and P Zhang, J. Phys.: Condens. Matter 24 (2012) 225801(10pp).

[34] H.M. Ledbetter and R.P. Reed, J. Phys. Chem., 2 (1973) 531-617.

[35] G.A. Slack, , Solid State Phys. 34 (1979) 1-71.

[36] S. Baroni, S. de Gironcoli, A. Dal Corso, and P. Giannozzi, Rev. Mod. Phys. 73 (2001) 515-62.

[37] A.A. Blanco, E. Francisco and V. Luana Comput. Phys. Commun. 158 (2004) 57-72.

[38] K. Bakker, E.H.P. Cordfunke, R.J.M. Konings, R.P.C. Schram, J. Nucl. Mater. 250 (1997) 1-12.

[39] B. Szpunar, J.A. Szpunar, Phys. Int. 4 (2013) 110-9.

[40] G.J. Hyland., J. Nucl. Mater., 113 (1983) 125-132.

[41] M. Samsel-Czekała, E. Talik, P. de V. Du Plessis, R. Troć, H. Misiorek, and C. Sułkowski, Phys. Rev. B 76 (2007) 144426 (16 pp).

[42] Q. Yin, A. Kutepov, K. Haule, and G. Kotliar, S.Y. Savrasov and W.E. Pickett, Phys. Rev. B84 (2011) 195111 (5pp).

[43] H. W. Knott, G. H. Lander, M. H. Mueller, and O. Vogt, Phys. Rev. B 21 (1980) 4159-65.

[44]P. Giannozzi, S. Baroni, N. Bonini, M. Calandra, R. Car, C. Cavazzoni, D. Ceresoli, G. L. Chiarotti, M. Cococcioni, I. Dabo, A. D. Corso, S. de Gironcoli, S. Fabris, G. Fratesi, R. Gebauer, U. Gerstmann, C. Gougoussis, A. Kokalj, M. Lazzeri, L. Martin-Samos, N. Marzari, F. Mauri, R. Mazzarello, S. Paolini, A. Pasquarello, L. Paulatto, C. Sbraccia, S. Scandolo, G. Sclauzero, A. P. Seitsonen, A. Smogunov, P. Umari, and R. M. Wentzcovitch, J. Phys.: Condens. Matter 21 (2009) 395502 (19pp).

[45] G.K.H. Madsen, D.J. Singh, Comput. Phys. Commun., 175 (2006) 67-71.

[46] T. Ohmichi, T. Kikuchi and S. Nasu, J. Nucl. Scie. Technol. 9 (1972) 77-85.

[47] J.A. Webb, I. Charit, J. Nucl. Mater, 427 (2012) 87-94.

[48] H. Muta, K. Kurosaki, M. Uno, S. Yamanaka, J Mater. Sci. 43 (2008) 6429–6434.